Science Advances
AAAS

advances.sciencemag.org/cgi/content/full/5/12/eaay1357/DC1

Supplementary Materials for

Recruitment of CD103$^+$ dendritic cells via tumor-targeted chemokine delivery enhances efficacy of checkpoint inhibitor immunotherapy

John-Michael Williford, Jun Ishihara, Ako Ishihara, Aslan Mansurov, Peyman Hosseinchi, Tiffany M. Marchell, Lambert Potin, Melody A. Swartz, Jeffrey A. Hubbell*

*Corresponding author. Email: jhubbell@uchicago.edu

Published 11 December 2019, *Sci. Adv.* **5**, eaay1357 (2019)
DOI: 10.1126/sciadv.aay1357

This PDF file includes:

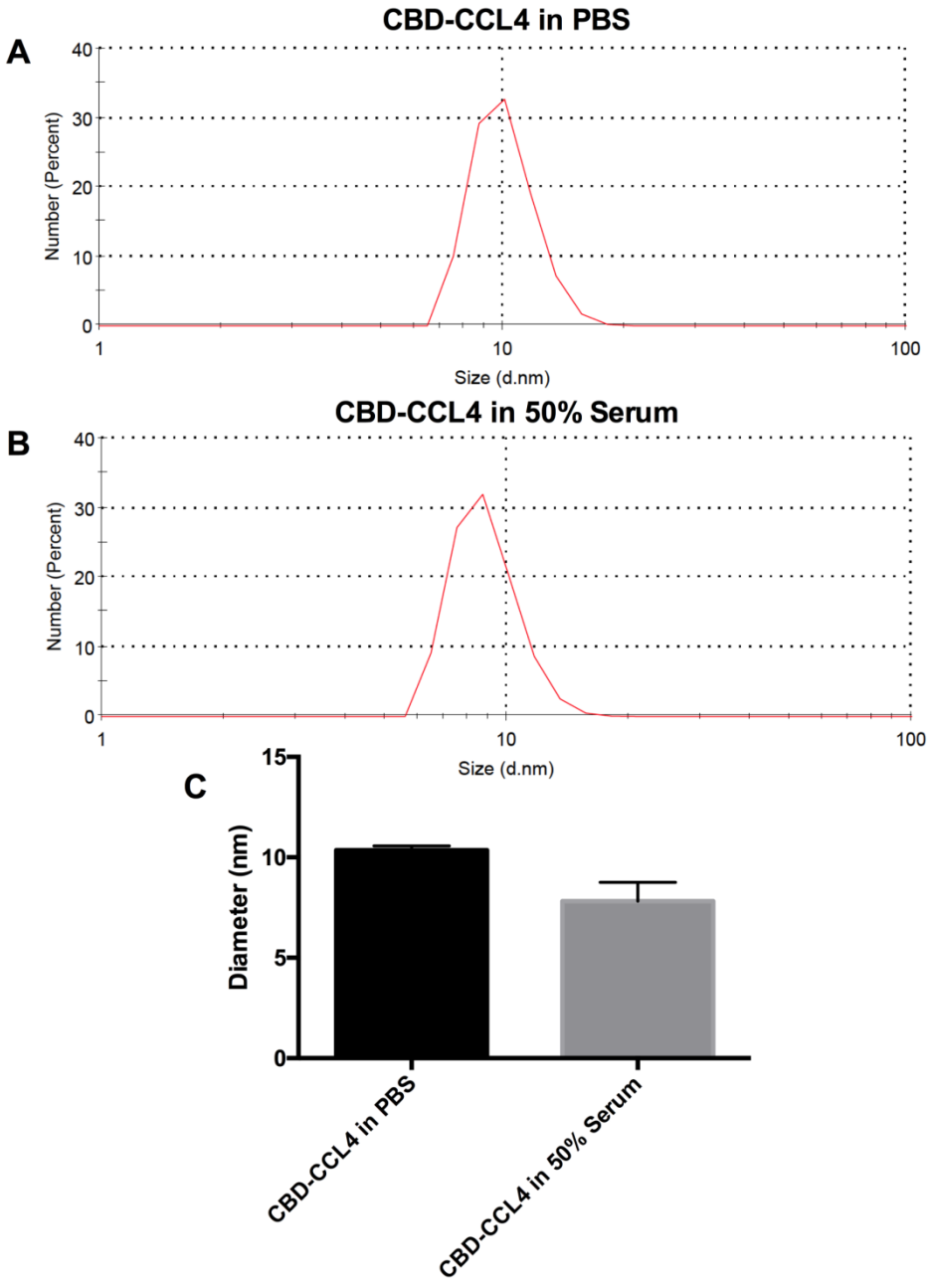

Fig. S1. Dynamic light scattering measurement of CBD-CCL4. Representative dynamic light scattering size distribution of CBD-CCL4 in (A) PBS and (B) 50% mouse serum; (C) comparison of average size of CBD-CCL4 measurements shown in (A) and (B). Bars represent mean ± SEM, n = 3.

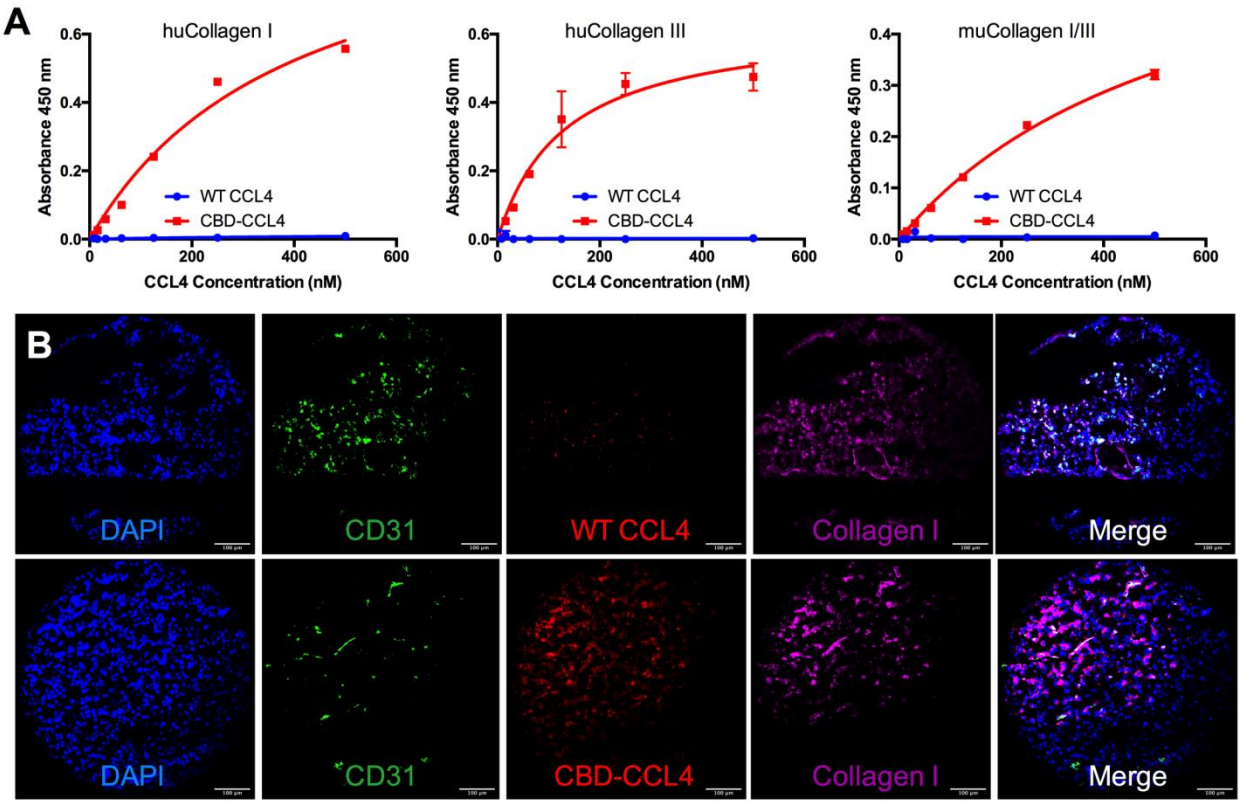

Fig. S2. Binding of CBD-CCL4 and WT CCL4 to collagen and murine melanoma sections.

(A) ELISA characterization of binding of WT CCL4 and CBD-CCL4 to human and murine collagen I and collagen III. (B) Binding of WT CCL4 or CBD-CCL4 to murine B16F10 melanoma cryosections as determined by immunofluorescence microscopy. All scale bars represent 100 μm.

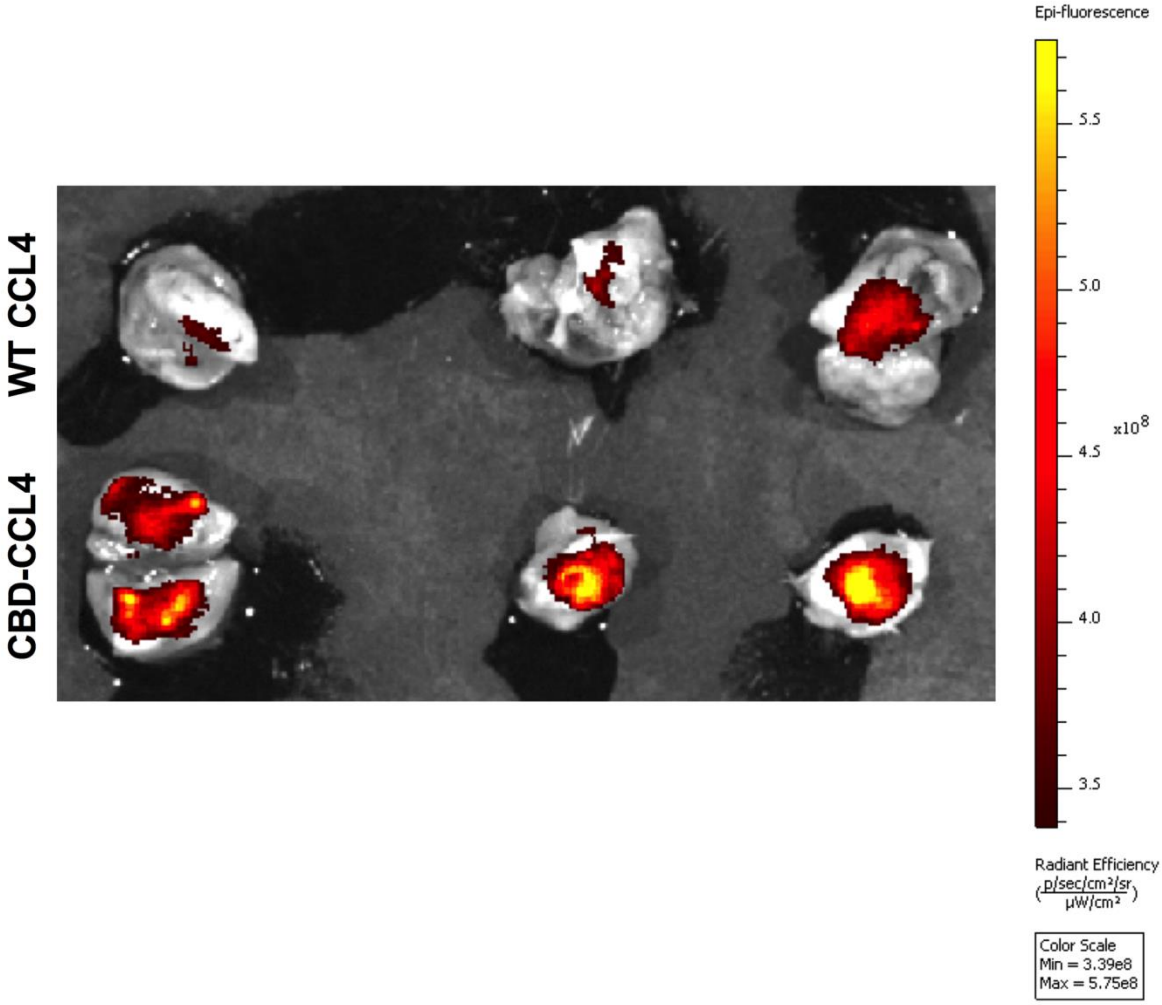

Fig. S3. In vivo imaging of EMT6 tumors. Fluorescent images of EMT6 tumors treated with WT CCL4 or CBD-CCL4 used to calculate tumor localization in Fig. 1H.

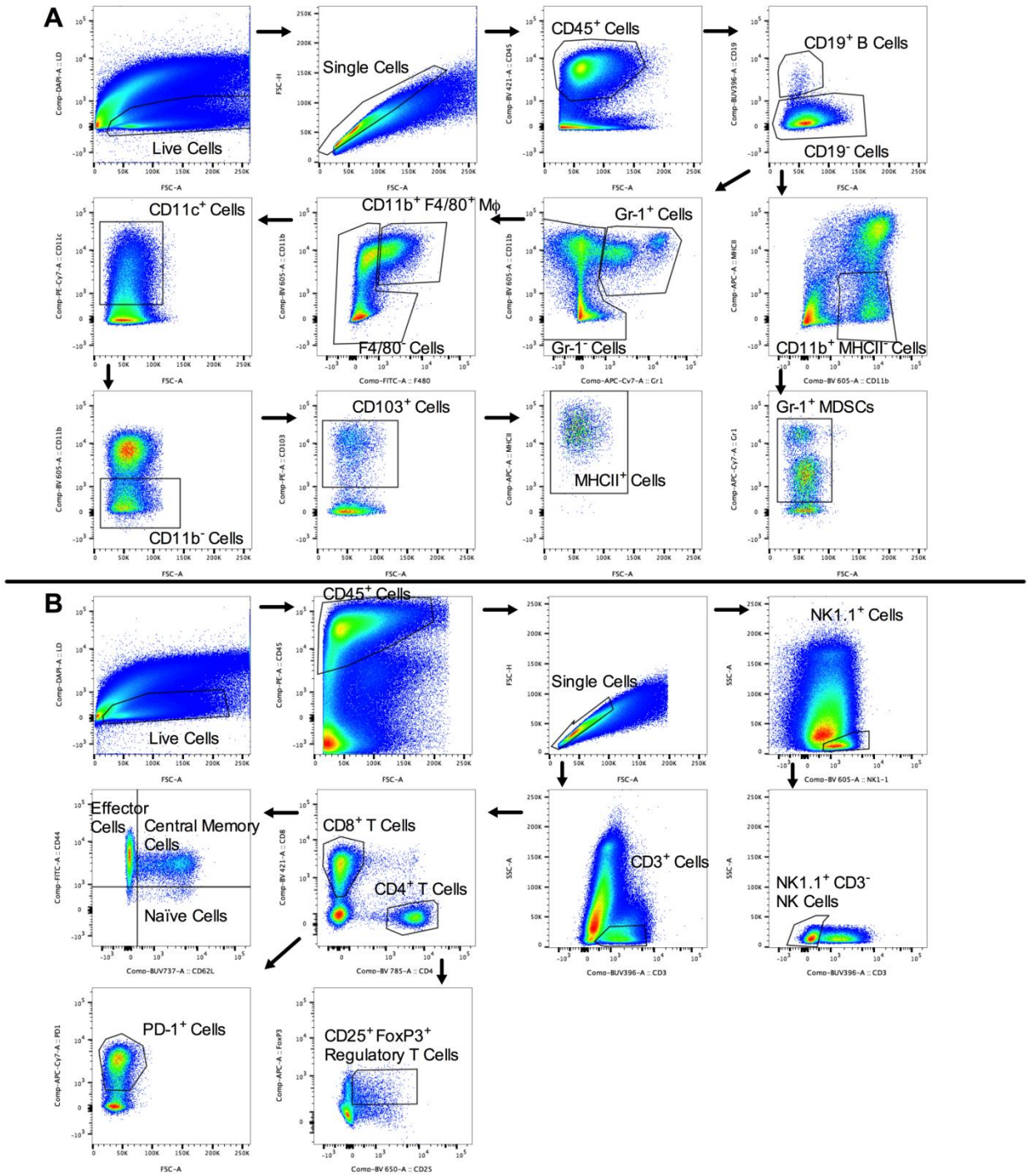

Fig. S4. Representative flow cytometry gating strategy. Gating strategies for flow cytometry analysis of (A) myeloid and (B) T cell immune cell infiltrates into tumors.

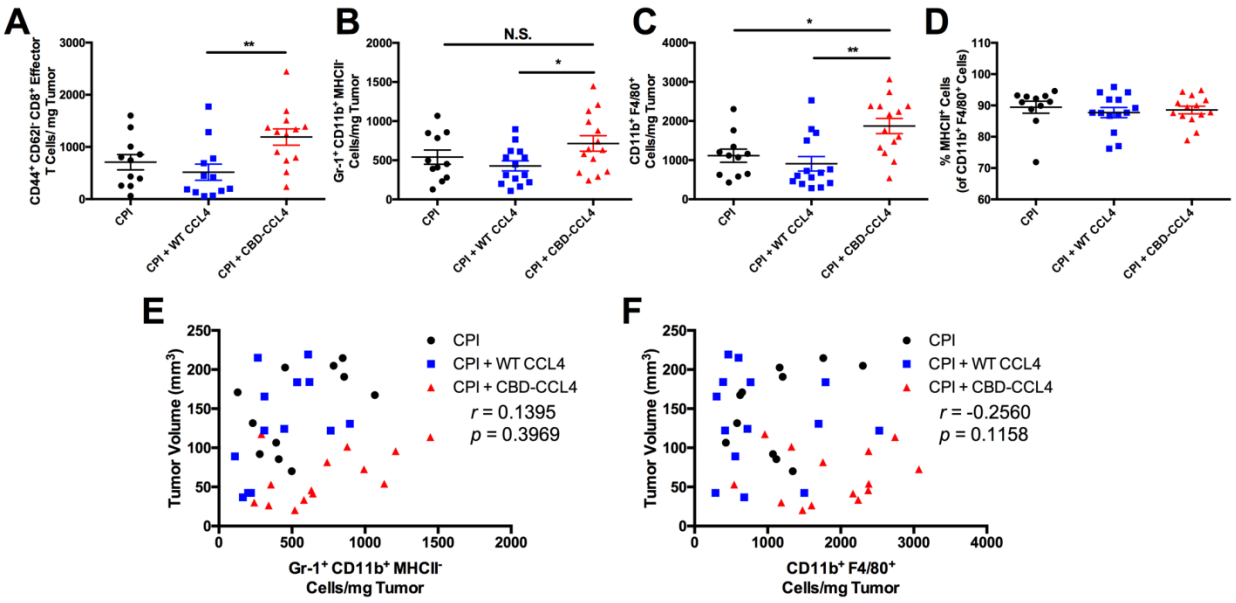

Fig. S5. Cell infiltrate analysis of effector T cells, MDSCs, and macrophages in B16F10 melanoma. Mice were intradermally injected with 5×10^5 cells; 4 d later, mice were treated with WT CCL4 (25 μg given via i.v. injection) or molar equivalent CBD-CCL4 (25 μg CCL4 basis, or 93 μg CBD-CCL4, given via i.v. injection) in combination with CPI antibody therapy consisting of 100 μg each αPD-L1 and αCTLA4 given via i.p. injection. CPI therapy alone was administered as control. (A-D) Immune cell infiltration was evaluated, where graphs depict the number of (A) $CD44^+$ effector $CD8^+$ T cells, (B) Gr-1^+ MDSCs, (C) $CD11b^+$ $F4/80^+$ macrophages and (D) $MHCII^+$ macrophages (of total $CD11b^+$ $F4/80^+$ cells). (E-F) Regression analysis comparing the number of tumor-infiltrating cells with tumor volume was performed using the results obtained in (B-C). Correlations between (E) tumor volume and Gr-1^+ MDSCs and (F) tumor volume and $CD11b^+$ $F4/80^+$ macrophages. Bars represent mean ± SEM, n = 11-13. *$p < 0.05$; **$p < 0.01$; N.S. not significant.

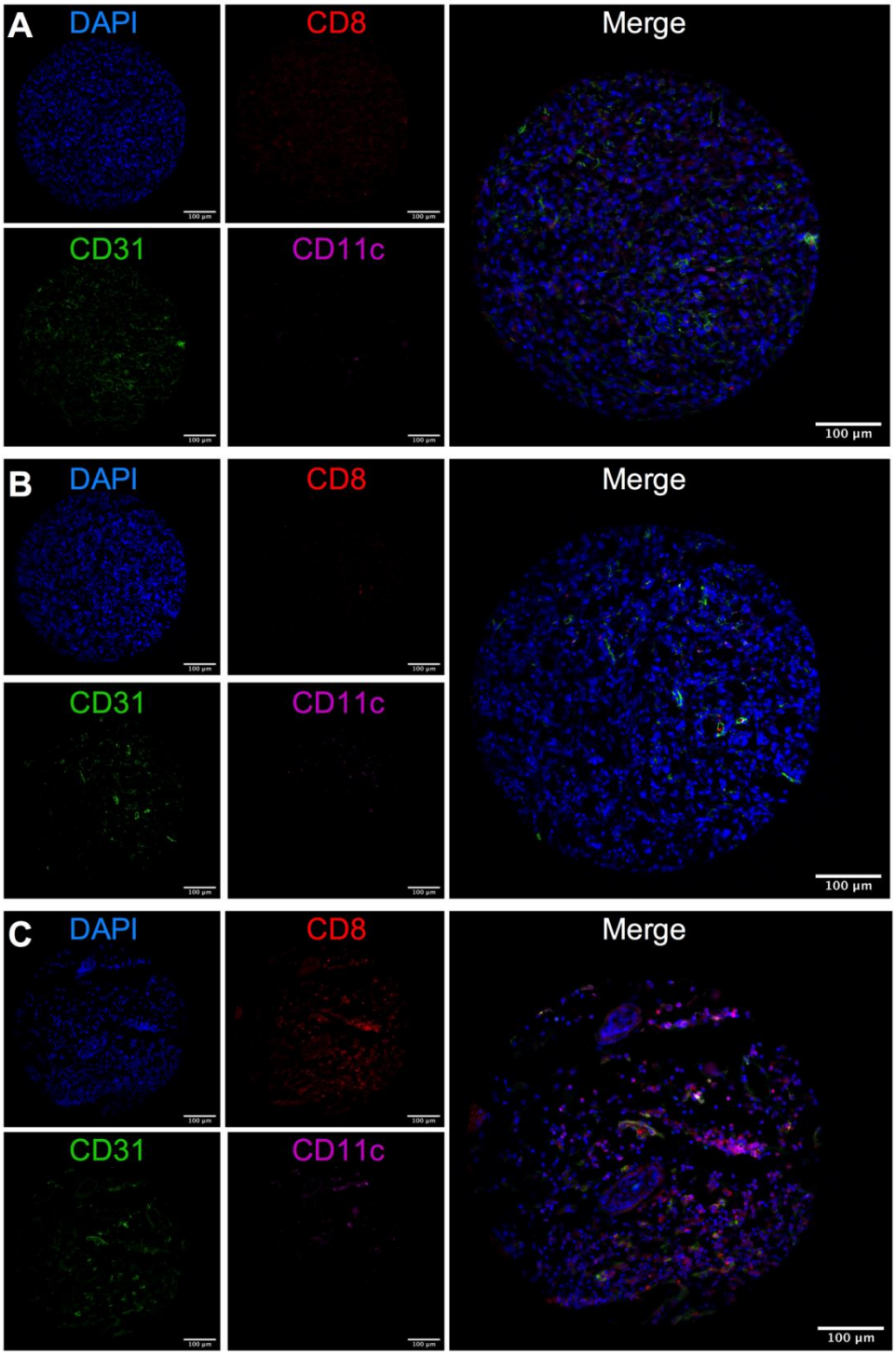

Fig. S6. Immunofluorescence analysis of $CD8^+$ cells and $CD11c^+$ DCs in EMT6 breast cancer. Mice were subcutaneously injected with 5×10^5 cells; 6 d and 9 d after inoculation, mice were treated with WT CCL4 (25 μg given via i.v. injection) or molar equivalent CBD-CCL4 (25

μg CCL4 basis, or 93 μg CBD-CCL4, given via i.v. injection) in combination with CPI antibody therapy consisting of 100 μg each αPD-L1 and αCTLA4 given via i.p. injection. CPI therapy alone was administered as control. Immune infiltration was evaluated by immunofluorescent microscopy following treatment with (A) CPI alone, (B) CPI + WT CCL4, and (C) CPI + CBD-CCL4. All scale bars represent 100 μm.

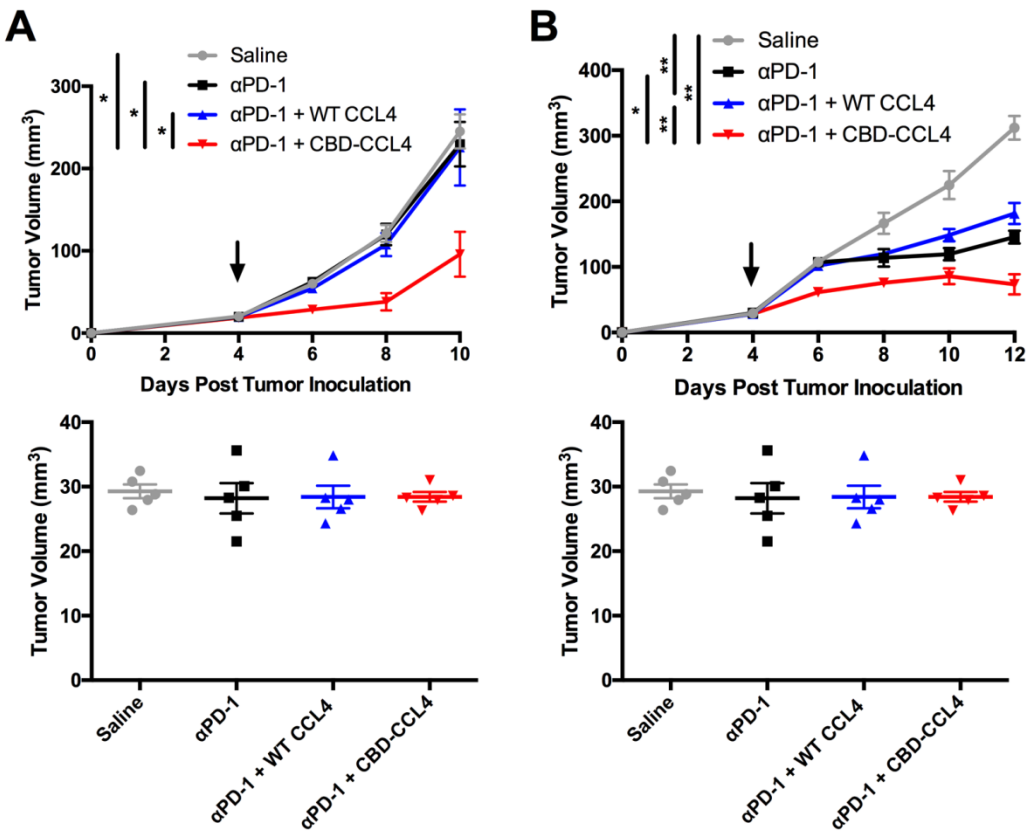

Fig. S7. Tumor growth curves of CT26 and MC38 following treatment with anti–PD-1 + CBD-CCL4. (A-B) Mice were intradermally injected with 5×10^5 CT26 or MC38 cells; 4 d after inoculation, mice were treated with WT CCL4 (25 μg given via i.v. injection) or molar equivalent CBD-CCL4 (25 μg CCL4 basis, or 93 μg CBD-CCL4 given via i.v. injection) in

combination with 100 μg αPD-1 given via i.p. injection. 100 μg αPD-1 alone was administered as control. Graphs depict growth curves and distribution of tumor sizes at time of treatment for (A) CT26 and (B) MC38 tumor models until the first mouse died. Bars represent mean ± SEM, n = 5. *$p < 0.05$; **$p < 0.01$. Arrows indicate time of treatment.

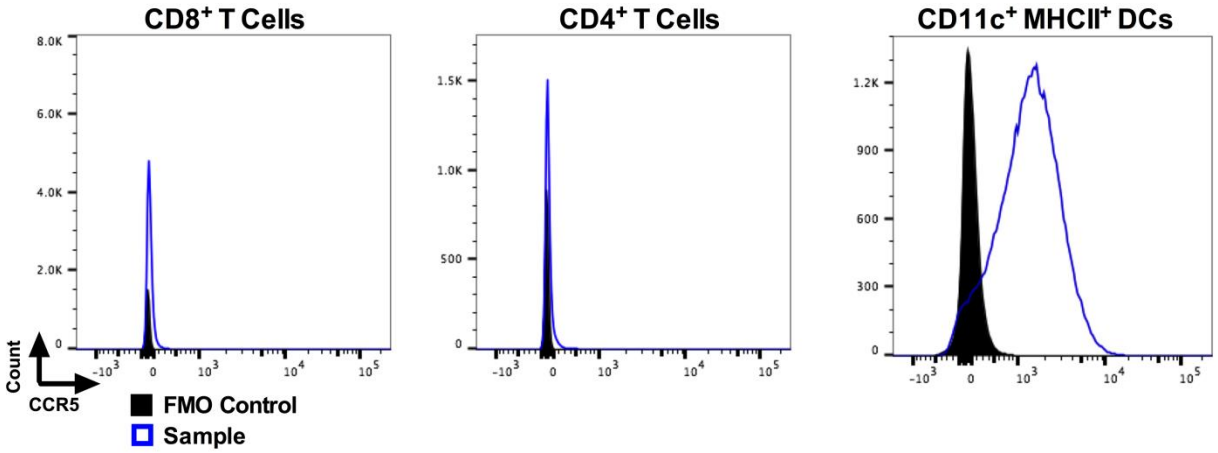

Fig. S8. CCR5 expression on T cells and DCs. Representative flow cytometry histograms depicting surface expression of CCR5 on $CD8^+$ T cells, $CD4^+$ T cells, and $CD11c^+$ $MHCII^+$ DCs.

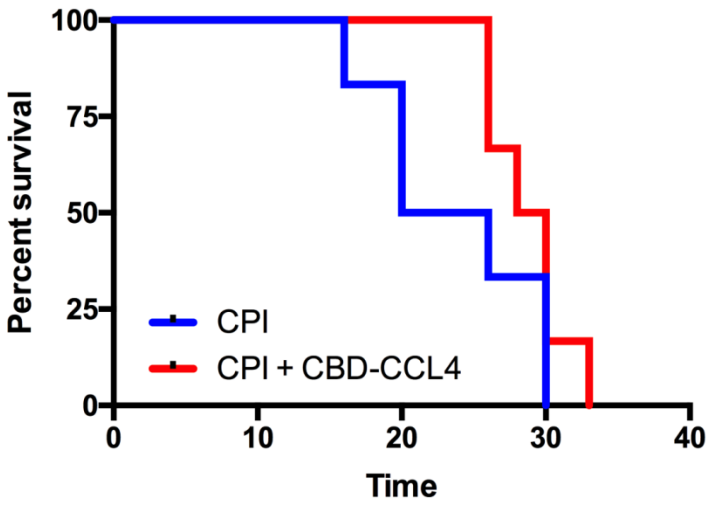

Fig. S9. Survival curves of spontaneous MMTV-PyMT mice following treatment.

Spontaneous MMTV-PyMT tumor-bearing mice were monitored until total tumor burden reached 100 mm^3. At this point, mice were treated with CBD-CCL4 (25 μg CCL4 basis, or 93 μg CBD-CCL4, given via i.v. injection) in combination with CPI antibody therapy consisting of 100 μg each αPD-L1 and αCTLA4 given via i.p. injection. CPI therapy alone was administered as comparison. Identical dosing was given 7 d and 14 d after the initial treatment. Graph depicts survival curves for each treatment group, n = 6

Table S1. Sequences of CCL4, CBD protein, and CBD-CCL4 fusion protein.

Murine CCL4 (WT CCL4)	A P M G S D P P T S C C F S Y T S R Q L H R S F V M D Y Y E T S S L C S K P A V V F L T K R G R Q I C A N P S E P W V T E Y M S D L E L N
Human VWF A3 domain (CBD protein)	C S Q P L D V I L L L D G S S S F P A S Y F D E M K S F A K A F I S K A N I G P R L T Q V S V L Q Y G S I T T I D V P W N V

	V P E K A H L L S L V D V M Q R E G G P S Q I G D A L G F A V R Y L T S E M H G A R P G A S K A V V I L V T D V S V D S V D A A A D A A R S N R V T V F P I G I G D R Y D A A Q L R I L A G P A G D S N V V K L Q R I E D L P T M V T L G N S F L H K L C S G F V R I
Human VWF A3 domain and murine CCL4 fusion protein (CBD-CCL4)	C S Q P L D V I L L L D G S S S F P A S Y F D E M K S F A K A F I S K A N I G P R L T Q V S V L Q Y G S I T T I D V P W N V V P E K A H L L S L V D V M Q R E G G P S Q I G D A L G F A V R Y L T S E M H G A R P G A S K A V V I L V T D V S V D S V D A A A D A A R S N R V T V F P I G I G D R Y D A A Q L R I L A G P A G D S N V V K L Q R I E D L P T M V T L G N S F L H K L C S G F V R I G G G G S G G G G S A P M G S D P P T S C C F S Y T S R Q L H R S F V M D Y Y E T S S L C S K P A V V F L T K R G R Q I C A N P S E P W V T E Y M S D L E L N H H H H H H